

## THE CENTRAL STAR OF THE PLANETARY NEBULA ABELL 78

JAMES B. KALER<sup>1,2</sup>

Astronomy Department, University of Illinois

AND

WALTER A. FEIBELMAN<sup>1</sup>

Laboratory for Astronomy and Solar Physics, NASA/Goddard Space Flight Center

Received 1983 November 21; accepted 1984 February 1

## ABSTRACT

We have studied the ultraviolet spectrum of the nucleus of Abell 78, one of the two planetaries known to contain zones of nearly pure helium. Although Abell 78 is strikingly similar in many respects to Abell 30, the other planetary with embedded helium knots, it differs in that there is only marginal evidence for absorption of starlight by circumstellar dust. The dust implied by the infrared emission is perhaps toroidally distributed about the star, with our view pole-on. This dissimilarity with Abell 30 may be related to the difference between nebular morphologies.

The ultraviolet-optical color temperature, which we tentatively identify with the effective temperature, almost certainly lies between 67,000 K and 130,000 K. The limitations are set primarily by the error in the interstellar extinction, as well as by uncertainty in the applicable model, and by the photometric precision of the *IUE*. The best two choices of extinction now available yield 77,000 and 84,000 K. From the current evolutionary tracks and distance, these temperatures imply a mass of 0.56–0.58  $M_{\odot}$  (from the best extinction values) with a possible full span of 0.55–0.7  $M_{\odot}$ . Comparison of the 77,000 K temperature with the He II Zanstra limit implies an optical depth of about 0.3 at the He<sup>+</sup> Lyman limit, if internal dust absorption is ignored.

The O v and N v P Cygni lines have terminal velocities similar to the value of 4200 km s<sup>-1</sup> measured earlier for C IV. A new possible P Cygni line is also seen at  $\lambda 1310$ , which we tentatively identify as Si II. There is no evidence for any significant change in the spectrum over a 5 year interval.

*Subject headings:* nebulae: individual — nebulae: planetary — stars: early-type — ultraviolet: spectra

## I. THE TWO PLANETARIES

Abell 30 and Abell 78 (208+33°1 and 81–14°1 in Perek and Kohoutek 1967), together with their central stars, exhibit remarkable characteristics, the most outstanding being the zones of nearly pure helium that are embedded within the main bodies of the nebulae. Hazard *et al.* (1980) found that a knot near the central star of A30 is devoid of detectable hydrogen. Jacoby and Ford (1983) extended the observations to other knots with the same result, and to the inner nebulosity in A78, which exhibits the same phenomenon.

Cohen *et al.* (1977, hereafter CHOS), showed from circumstellar emission in the near infrared that the stars are surrounded by dust clouds embedded in the nebulae, which provides evidence for mass loss. Direct evidence for a wind has come from observations made with the *International Ultraviolet Explorer* (*IUE*). Heap (1979) found very strong P Cygni profiles of C IV at  $\lambda 1550$ , O v at  $\lambda 1371$ , and N v at  $\lambda 1240$  in A78's central star spectrum. Greenstein (1981) discovered very similar features in the nucleus of A30. He also found further evidence for circumstellar dust in A30 from anomalous absorption in the ultraviolet that lacked the characteristic  $\lambda 2200$  Å feature, and he hypothesized a dust of carbon smoke.

<sup>1</sup> Guest Observers with the *International Ultraviolet Explorer* satellite, which is sponsored and operated by the National Aeronautics and Space Administration, by the Science Research Council of the United Kingdom, and by the European Space Agency.

<sup>2</sup> Visiting Astronomer, Kitt Peak National Observatory, which is operated by the Association of Universities for Research in Astronomy, Inc., under contract with the National Science Foundation.

Apparently some of the heavier atoms are condensing out of the winds to form grains, which, from the extent of the infrared emission, occur within about 0.1 pc of the stars, roughly coincident with the zones of high helium content.

In Table 1 we present various properties of the nebulae and their nuclei, modified from Kaler (1983) for the dust extinctions given by CHOS ( $c = 0.42$  for A30,  $c = 0.18$  for A78, where  $c$ , the logarithmic absorption at  $H\beta$ , is equal to  $0.47 A_v$  and  $1.41 E_{B-V}$  for the Whitford (1958) interstellar extinction function). These parameters emphasize the similarity of the objects. The second and third rows show that both nebulae are very large, with comparable excitation as

TABLE 1  
PROPERTIES OF ABELL 30 AND ABELL 78

| Property                                   | Abell 30          | Abell 78            |
|--|-------------------|---------------------|
| Distance (kpc) .....                       | 1.41              | 1.63                |
| Radius (pc) .....                          | 0.44              | 0.43                |
| $I(\lambda 4686)$ He II <sup>a</sup> ..... | $152 \pm 7$       | $187 \pm 54$        |
| $10^3 T_e(\text{H})$ (K) .....             | $> 25 \pm 1$      | $> 22 \pm 1$        |
| $L_z(\text{H})$ ( $L_{\odot}$ ) .....      | $> 53 \pm 3$      | $> 89 \pm 7$        |
| $10^3 T_e(\text{He II})$ (K) .....         | $\geq 73 \pm 1$   | $\geq 69 \pm 2$     |
| $L_z(\text{He II})$ ( $L_{\odot}$ ) .....  | $\geq 880 \pm 60$ | $\geq 1620 \pm 190$ |
| $R_*$ ( $R_{\odot}$ ) .....                | $\leq 0.19$       | $\leq 0.28$         |
| $\log g$ .....                             | $\geq 5.6$        | $\geq 5.3$          |
| P Cyg features .....                       | C IV, N v, O v    | C IV, N v, O v      |
| $v_{\infty}$ (km s <sup>-1</sup> ) .....   | $\sim 4000$       | $\sim 4200$         |

<sup>a</sup>  $I(H\beta) = 100$ .

expressed by similar integrated  $I(\lambda 4686 \text{ He II})/I(\text{H}\beta)$  ratios, implying the same central star temperatures and luminosities. The close pairing of the stars' optical spectra was noted many years ago by Greenstein and Minkowski (1964), who classified them both as O5f, with strong O VI features. The next four rows give the Zantra temperatures and luminosities. The low hydrogen Zantra temperatures [ $T_z(\text{H})$ ] imply that the nebulae are optically thin in the hydrogen Lyman ultraviolet, although some of the depression may be due to the circumstellar dust that absorbs ionizing photons (Helfer *et al.* 1981). The powerful  $\lambda 4686 \text{ He II}$  lines indicate low optical depth in the  $\text{He}^+$  Lyman UV (see Kaler 1983), showing that the  $\text{He II}$  temperatures [ $T_z(\text{He II})$ ] and luminosities are also lower limits. From these, the calculated stellar radii ( $R_*$ ), which are upper limits, are within a factor of 2 of one another. The lower limits to the surface gravities,  $g$ , calculated from  $R_*$  and masses of  $0.55 M_\odot$  indicated by their placement limits on the  $\log L$ - $\log T$  plane (see Kaler 1983), are also similar. Finally, Kaler and Feibelman (1984, hereafter KF) determined an approximate terminal velocity ( $v_\infty$ ) of  $4200 \text{ km s}^{-1}$  for A78 from C IV, and from Greenstein's (1981) Figure 1, we infer here very roughly that  $v_\infty$  for A30 is not much different. From all the data—the helium zones, infrared emission, and P Cygni profiles—the mass loss processes in the two stars must be nearly identical, consistent with the other similar stellar properties.

From an evolutionary point of view, it would appear that each star has lost any hydrogen envelope that remained after the formation of the main body of the planetary, leaving a bare helium core that it is now in the process of driving off. Iben *et al.* (1983) suggest that these two stars, and perhaps some of the others listed by Kaler (1981), are repeating their evolutionary paths, after having suffered a final thermal pulse during their initial passages through the planetary domain of the  $\log L$ - $\log T$  plane. They maintain that the stars are now on the horizontal, high-luminosity portions of the tracks (where we would expect small, younger objects) with large radii that suggest that they are relatively old. This idea is also supported by the low velocities found for the A30 knots by Reay, Atherton, and Taylor (1983), which are appropriate to mass ejection during a brief postpulse giant phase.

There are some interesting differences between the two objects, however. Both nebulae exhibit a limb-brightened, or ring, structure, but from G. H. Jacoby's (private communication) photographs, that of A78 is more pronounced and is broken into two rather distinct portions that are arranged in a more ellipsoidal fashion. This difference can also be seen on the Palomar Sky Survey photos reproduced by Kaler (1981). There is also distinct contrast in the extinction to the pair. The nucleus of A30 is heavily reddened, which from consideration of the high galactic latitude ( $31^\circ$ ) and the ultraviolet spectrum, is caused by circumstellar dust (Greenstein 1981). This conclusion is confirmed by the absence of interstellar extinction to the nebula (Kaler 1981). The reddening of the A78 nucleus, however, is more consistent with an interstellar origin, with  $A_v = 0.39 \text{ mag}$  from CHOS compatible with  $b = 14^\circ$  and well within the error of Kaler's (1983) uncertain nebular extinction.

For tests of existing, and for the development of new, evolution theory, it is imperative that the effective temperatures and luminosities of these and similar stars be measured properly. We are using the *IUE* to derive such values, or at

TABLE 2  
*IUE* OBSERVING LOG FOR ABELL 78

| Number          | Date        | Exp. Time (minutes) | Saturation                      |
|-----------------|-------------|---------------------|---------------------------------|
| SWP 13351 ..... | 1981 Mar 22 | 12                  | $\lambda 1240$ – $\lambda 1380$ |
| LWR 10189 ..... | 1981 Mar 22 | 30                  | $\lambda 2430$ – $\lambda 2980$ |
| SWP 16966 ..... | 1982 May 15 | 6                   | ...                             |
| LWR 13250 ..... | 1982 May 15 | 12                  | ...                             |
| SWP 19907 ..... | 1983 May 5  | 4                   | ...                             |
| LWR 15881 ..... | 1983 May 5  | 6                   | ...                             |

least likely ranges, directly from the ultraviolet energy distributions. A survey of the results from the stars observed so far by KF shows a wide range of stellar properties and color temperatures. Here we begin to look in detail at individual stars, starting with the one in A78. In the sections below we will examine the line spectrum and wind velocities, improve the determination of interstellar extinction for an assessment of circumstellar dust, and then derive the temperature, luminosity, and core mass. The heavy anomalous reddening of the A30 nucleus precludes a temperature determination by this means. But because of the general similarity between A78 and A30, we might logically assign the temperature found for the former to the latter, for a more definite evaluation of the odd circumstellar dust.

## II. THE OBSERVATIONS

All observations of the nucleus of A78 were made with the large aperture at low dispersion. We took three exposures each with the SWP and LWR cameras, with different integration times, in order to provide a range of photon counts at all wavelengths. Exposure numbers, dates, exposure times, and regions of saturation are shown in the observing log, Table 2. The data were reduced by standard *IUE* procedures, which include extrapolations in saturated spectral regions. The background nebulae have such low surface brightness that they are of no consequence whatever.

We show the two longer exposure reduced SWP spectra in Figure 1, and the 12 minute LWR spectrum in Figure 2. The longest LWR exposure was badly saturated between  $\lambda 2500$  and  $\lambda 2800$  and is not suitable for illustration. The spectra rise rapidly to the short ultraviolet, as befits such a hot source as a high-excitation planetary nucleus, and are dominated by the three powerful P Cygni lines first pointed out by Heap (1979):  $\lambda 1550 \text{ C IV}$ ,  $\lambda 1371 \text{ O V}$ , and  $\lambda 1240 \text{ N V}$ . Comparison of the three SWP spectra, and of these with Heap's, show that no significant changes have taken place over the 5 year period from 1978 to 1983.

A weak feature is visible at  $\lambda 1310$  on both of the displayed SWP spectra, and thus it is probably real. It does not appear on the shortest exposure, but that may be simply a result of the decreased signal-to-noise ratio. It is too weak for us to be certain that it is another P Cygni line, but by analogy it probably is. The identification is unsure. It coincides with  $\lambda 1310 \text{ Si II}$  (see Adelman, Adelman, and Fischel 1977), but the high excitation of the rest of the spectrum and of the nebula cast doubt on such a conclusion. There is no evidence for the  $\lambda 1320 \text{ O IV}$  or  $\lambda 1640 \text{ He II}$  lines identified by Heap (1979).

All three LWR spectra show some evidence for an absorption line at  $\lambda 2905$ , which is coincident with  $\lambda 2905.3$  of  $\text{Si IV}$  (Kelly 1979). However, the much stronger  $\text{Si IV}$

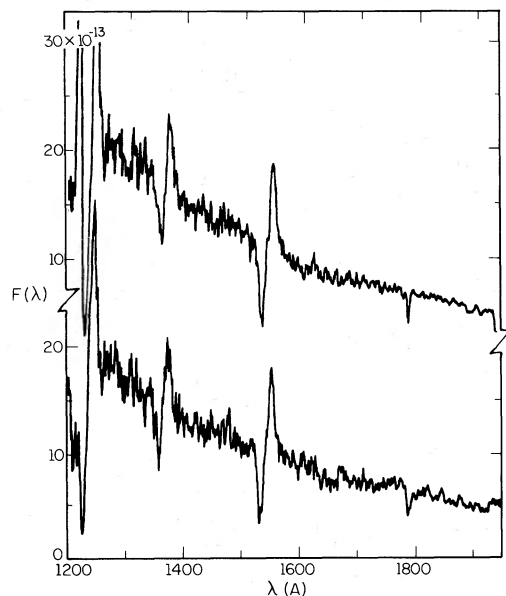


FIG. 1.—The two longer exposure SWP spectra of the nucleus of Abell 78. The three strong P Cygni lines are  $\lambda 1240$  N v,  $\lambda 1371$  O v, and  $\lambda 1550$  C iv. A weak feature, which appears to be real, is seen on both spectra at  $\lambda 1310$ . The feature at  $\lambda 1790$  is a reseau mark.

lines at  $\lambda 3150$  and  $\lambda 3167$  are not present. The broad interstellar absorption bump at  $\lambda 2200$ , from which we derive the interstellar extinction below, is clearly evident in Figure 2.

We tabulate the mean observed continuum fluxes in column (4) of Table 3, where we smoothed the spectrum and selected sample points every  $50 \text{ \AA}$ . We also smoothed through the P Cygni features, and give the continuum we would expect were no lines present; see footnote b. The individual fluxes from each exposure were weighted proportionately with exposure time (3:2:1 and 4:2:1 for the SWP and LWR, respectively, in chronological order), excluding the two saturated regions in the March 22 data. The results of this paper are virtually unchanged if we adopt a straight mean.

Comparison of the four exposures indicates two problems with systematic error in the IUE data. First, the fluxes at each wavelength are exposure dependent. As we proceed toward shorter SWP integration times, the fluxes drop by an

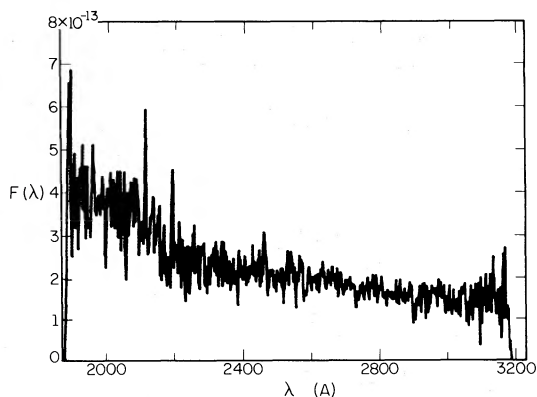


FIG. 2.—The second (medium-exposure) LWR spectrum of the nucleus of Abell 78, which shows the weak interstellar absorption feature at  $\lambda 2200 \text{ \AA}$ .

average of about 5% from one exposure to the next. Similar differences are seen by KF for several other pairs of SWP exposures of other stars. The LWR region is more complicated. Between  $\lambda 2000$  and  $\lambda 2400$ , the fluxes increase by an average of 5% on going from the 30 to the 12 minute exposure, and then drop by about 10% from the latter to the 6 minute exposure. Between  $\lambda 2400$  and  $\lambda 3000$ , the ratio of  $F(12 \text{ minutes})$  to  $F(6 \text{ minutes})$  varies between 0.87 and 1.15. We cannot entirely rule out small stellar variations, but the problem is likely to be intrinsic to the IUE, especially in view of the second problem, which occurs in the region of overlap between the SWP and LWR spectra. The ratios of  $F_{\lambda}(\text{SWP})/F_{\lambda}(\text{LWR})$  for  $\lambda 1900$  and  $\lambda 1950$  for each pair of exposures made on each of the three dates average 1.18.

TABLE 3  
THE ENERGY DISTRIBUTION OF THE CENTRAL STAR OF ABELL 78

| $\lambda$<br>(1)  | $f_{\lambda}$<br>(2) | $f_{\lambda}(\text{A30})$<br>(3) | $10^{13} F_{\lambda} d_{\lambda}$ |                               |
|-------------------|----------------------|----------------------------------|-----------------------------------|-------------------------------|
|                   |                      |                                  | Observed<br>(4)                   | Corrected <sup>a</sup><br>(5) |
| 1250              | 1.61                 | 0.66                             | 18.7                              | 52.7                          |
| 1300 <sup>b</sup> | 1.49                 | 0.60                             | 17.0                              | 45.7                          |
| 1350              | 1.37                 | 0.49                             | 15.1                              | 38.6                          |
| 1400              | 1.29                 | 0.47                             | 14.3                              | 35.5                          |
| 1450              | 1.24                 | 0.40                             | 12.6                              | 30.6                          |
| 1500              | 1.20                 | 0.40                             | 11.6                              | 27.8                          |
| 1550 <sup>b</sup> | 1.20                 | 0.39                             | 10.5                              | 25.1                          |
| 1600              | 1.20                 | 0.38                             | 9.09                              | 21.7                          |
| 1650              | 1.17                 | 0.37                             | 8.14                              | 19.2                          |
| 1700              | 1.13                 | 0.37                             | 7.63                              | 17.8                          |
| 1750              | 1.11                 | 0.38                             | 7.23                              | 16.7                          |
| 1800              | 1.10                 | 0.45                             | 6.61                              | 15.3                          |
| 1850              | 1.12                 | 0.51                             | 5.98                              | 13.9                          |
| 1900              | 1.17                 | 0.58                             | 4.96                              | 11.7                          |
| 1950              | 1.25                 | 0.61                             | 4.61                              | 11.3                          |
| 2000              | 1.35                 | 0.64                             | 3.85                              | 9.82                          |
| 2050              | 1.45                 | 0.67                             | 3.47                              | 9.20                          |
| 2100              | 1.53                 | 0.69                             | 3.22                              | 8.81                          |
| 2150              | 1.60                 | 0.72                             | 2.87                              | 8.07                          |
| 2200              | 1.62                 | 0.75                             | 2.47                              | 7.00                          |
| 2250              | 1.52                 | 0.82                             | 2.38                              | 6.51                          |
| 2300              | 1.40                 | 0.92                             | 2.31                              | 6.06                          |
| 2350              | 1.28                 | 0.94                             | 2.24                              | 5.62                          |
| 2400              | 1.17                 | 0.95                             | 2.18                              | 5.24                          |
| 2450              | 1.06                 | 0.96                             | 2.18                              | 5.03                          |
| 2500              | 0.98                 | 0.96                             | 2.13                              | 4.77                          |
| 2550              | 0.90                 | 0.96                             | 2.11                              | 4.59                          |
| 2600              | 0.84                 | 0.96                             | 2.06                              | 4.38                          |
| 2650              | 0.77                 | 0.95                             | 1.99                              | 4.12                          |
| 2700              | 0.72                 | 0.93                             | 1.81                              | 3.67                          |
| 2750              | 0.68                 | 0.90                             | 1.70                              | 3.39                          |
| 2800              | 0.64                 | 0.85                             | 1.62                              | 3.18                          |
| 2850              | 0.60                 | 0.79                             | 1.57                              | 3.03                          |
| 2900              | 0.57                 | 0.76                             | 1.50                              | 2.86                          |
| 2950              | 0.53                 | 0.72                             | 1.48                              | 2.78                          |
| 3000              | 0.51                 | 0.69                             | 1.44                              | 2.57                          |
| 3050              | 0.48                 | 0.60                             | 1.30                              | 2.39                          |
| 3100              | 0.46                 | 0.63                             | 1.25                              | 2.28                          |
| 3333 <sup>c</sup> | 0.38                 | 0.43                             | 0.927                             | 1.63                          |
| 4400 <sup>d</sup> | 0.12                 | 0.12                             | 0.375                             | 0.592                         |
| 5000              | -0.03                | -0.03                            | 0.247                             | 0.367                         |
| 5500              | -0.10                | -0.14                            | 0.178                             | 0.253                         |
| 6600              | -0.24                | -0.34                            | 0.096                             | 0.126                         |

NOTE.—Units for cols. (4) and (5):  $\text{ergs cm}^{-2} \text{ s}^{-1} \text{ \AA}^{-1}$ .

<sup>a</sup>  $c = 0.164$ ,  $c(\text{A30}) = 0.13$ .

<sup>b</sup> Continuum smoothed through P Cygni features.

<sup>c</sup> Flux for  $\lambda = 3333$  from Greenstein (1983).

<sup>d</sup> Fluxes for  $\lambda \geq 4400 \text{ \AA}$  from Cohen *et al.* (1977) and Greenstein (1983).

Bohlin and Holm (1980) address this difficulty and claim that the match-up between the SWP and LWR is now fixed in the reduction procedure, but from our spectra there still seems to be some error, opposite in direction to that which existed before the revision in the reduction program. If for the sake of later analysis we consider all of the above variations to be random, we then calculate an internal mean error to the mean fluxes in Table 3 of  $\pm 3\%$ .

The *IUE* data are given through  $\lambda 3100$ . In order to provide a long wavelength base it is necessary to include a sample of stellar optical fluxes. We choose them at  $\lambda 3333$  from Greenstein (1983), and at  $\lambda 4400$ , 5000, 5500, and 6600 from an average of his and CHOS's observations. Greenstein (1983) uses the new calibration of Oke and Gunn (1983). CHOS do not give their calibration source, so that no attempt is made to place them on the same system, and the data are accepted as given. The mean error derived from the differences between the two sets of data is  $\pm 2\%$ . The combined ultraviolet-to-optical uncertainty is then taken to be  $\pm 3.5\%$ .

### III. ANALYSIS

#### a) Terminal Velocities

KF give a terminal wind velocity of  $4200 \text{ km s}^{-1}$  from measurements of  $\lambda 1550 \text{ C IV}$  on all three SWP spectra. The derivation of  $v_\infty$  from the low-dispersion exposures can here only be approximate because the instrumental line width is comparable to the observed emission- or absorption-line widths. KF used an average of the velocity derived from the confluence of the absorption component with the continuum, and that found from the separation of the emission and absorption components, a procedure which, though crude, should be a reasonable approximation to the true terminal velocity. A similar analysis of the  $\lambda 1371 \text{ O V}$  line yields  $4300 \text{ km s}^{-1}$ . The  $\lambda 1240 \text{ N V}$  line is confused with geocoronal  $\text{Ly}\alpha$ ; the line separation averages  $10\%$  larger than that for  $\lambda 1550 \text{ C IV}$ , which suggests a terminal velocity of about  $4600 \text{ km s}^{-1}$ . Differences among the three ions are not significant given the large but unknown error.

#### b) Interstellar and Circumstellar Extinction

In order to derive an effective temperature for the star, we must first accurately correct the data for reddening. Greenstein (1981) could not do so for A30 because the dust is circumstellar and of an odd nature. There is no external means of estimating the line-of-sight density of the dust for that star, and in order to study its effect, we must first adopt a temperature. The extinction to A78 seems to be dominantly of an interstellar nature, however. The optical reddening is much lower, and the UV spectrum exhibits the  $\lambda 2200$  feature with no evidence for the broad absorption at  $\lambda 2470$  associated with A30.

In all our work, we adopt an interstellar extinction function that is a composite of the ultraviolet curve of Savage and Mathis (1978) and the optical curve of Whitford (1958). This function,  $f_\lambda$ , is given in column (2) of Table 3 and is scaled such that  $f_{\text{H}\beta} = 0$  and  $f_\infty = -1$ , in accord with standard nebular practice.

The simplest way to measure the interstellar extinction, which we shall now characterize by  $c$ , the logarithmic extinction at  $\text{H}\beta$  (see § I), is by its effect on the nebular  $\text{H}\alpha/\text{H}\beta$  ratio. Kaler (1981) measured  $c = 0.04 \pm 0.42$  for A78

from wide-aperture filter photometry, but the error is too large for the value to be of much use, and the study by Jacoby and Ford (1983) concentrated on the helium zone, where the hydrogen lines are not seen. Thus we must rely on analysis of the star's observed energy distribution and the  $\lambda 2200$  feature.

Derivation of a precise extinction from the  $\lambda 2200$  bump is not a trivial matter. The feature extends from  $\approx \lambda 1800$  to  $\approx 2400$  and thus spans the overlapping regions of the LWR and SWP cameras, where the *IUE* calibration still appears to be uncertain (see the previous section). Thus, we must somehow recalibrate this spectral region for the purpose of extinction measurement. To do so, we used our similar observations of NGC 7094 (see KF), for which an accurate extinction is available from measurements made at Kitt Peak with the Intensified Reticon and Image Dissector Scanners (IRS and IIDS; Kaler 1983 and unpublished). From the IRS data on  $\text{H}\alpha$ ,  $\text{H}\beta$ , and  $\text{H}\gamma$ , where we give the  $\text{H}\alpha/\text{H}\beta$  ratio triple weight, we find  $c = 0.185$ , and from the IIDS measurements of  $\text{H}\alpha$  and  $\text{H}\beta$  we obtain  $c = 0.141$ . We assign double weight to the former because of a higher signal-to-noise ratio, and obtain  $\bar{c} = 0.171 \pm 0.02$  for NGC 7094. Because of the sensitivity of the derived temperature to extinction, and to avoid round-off errors, we will continue to carry  $c$  to three significant figures, in spite of whatever the errors might be.

We sampled the spectrum of the central star of NGC 7094 every  $10 \text{ \AA}$  between  $\lambda 1800$  and  $\lambda 2400$ . To the observed spectrum we fit a sequence of reddened blackbodies at  $100,000 \text{ K}$  (from KF) by averaging the ratios  $F(\text{observed})/F(\text{theoretical})$  at each point, and scaling the theoretical to the observed. The correct value of  $c$  is considered to be that which produces the minimum value of the sum of the squares of the percentage deviations ( $d$ ),

$$\sum \left[ \frac{F(\text{observed}) - F(\text{theoretical})}{F(\text{observed})} \right]^2 = \sum d^2. \quad (1)$$

Ideally, the derived  $c$  should be independent of the wavelength interval over which the fit is made, but systematic errors in the *IUE* reduction can cause it to vary rather widely. For our test case of NGC 7094,  $c$  equals 0.25 from a fit between  $\lambda 1800$  and  $\lambda 2400$ , (where we exclude the unreliable region  $\lambda 1910$ – $1940$ ), and 0.14 and 0.13 for fits between  $\lambda 2000$  and  $\lambda 2400$  and  $\lambda 2200$  and  $\lambda 2400$ . We found that the optical value of  $c = 0.171$  was matched if we averaged these three values, from which we find  $\bar{c}$  ( $\lambda 2200$  bump, NGC 7094) =  $0.171 \pm 0.04$ . The correction factor to be applied to  $c(\lambda 2200)$  to match the optical value is then taken to be  $1.00 \pm 0.25$ .

We apply this empirical compensating technique to the ultraviolet data acquired for A78, where we again weight the three exposures as described previously and adopt a blackbody temperature of  $77,000 \text{ K}$  (as determined from an iterative solution; see § IIIc). We then find  $c = 0.164$ , with an internal error of  $\pm 0.015$ , and a full error, which includes the uncertainty in the NGC 7094 analysis, of  $\pm 0.045$ . This value is consistent with Kaler's (1983) optical value and with the galactic latitude of  $14^\circ$ , and there is little indication that it is due to anything but interstellar dust. It is however, now very important to determine an accurate value of  $c$  from the  $\text{H}\alpha/\text{H}\beta$  ratio of the outer nebula.

The analysis of the optical spectrum yields a somewhat higher value. From CHOS's fluxes at  $\lambda 4400$ , 5000, 5500, and 6600, Greenstein's (1983) data between  $\lambda 4000$  and  $\lambda 9000$ , and

an assumed 77,000 K blackbody, we find  $\bar{c}$ (optical) to be  $0.177 \pm 0.012$ , where the error simply reflects the difference between  $c$ (CHOS) and  $c$ (Greenstein). Although the difference between  $c$  derived from  $\lambda 2200$  and that found from the optical is certainly marginal (from the errors between 0 and 0.070, with a most likely value of 0.013), it is in the same direction as the difference found for A30, where the optical color yields an extinction much higher than that expected for  $b = 33^\circ$ , and where there is no  $\lambda 2200$  bump at all.

If the difference in the two values of extinction found for A78 is real, which is problematical, it might be ascribed to a small amount of circumstellar dust with a character similar to that found for Abell 30. To be completely consistent, we assumed that the true flux distribution was reddened by both the interstellar function and the circumstellar function derived from Greenstein's (1981) data on A30 for  $T = 10^5$  K, here called  $f_\lambda$ (A30), which is given in column (3) of Table 3. Since  $f_\lambda$ (A30) is fairly flat through the ultraviolet, its addition has little effect on the analysis of the  $\lambda 2200$  bump. Since the circumstellar extinction constant  $c$ (A30) is small, and since  $f_\lambda$ (A30) does not differ much from the Whitford function,  $c$ (A30) simply equals the difference between the optical and the  $\lambda 2200$  ultraviolet extinctions, or 0.013 (+0.051, -0.013), where the error includes an iteration with temperature. This is clearly a marginal result, one that sets a rather stringent limit on the amount of circumstellar dust in the line of sight. We refer to this concept below as the "basic extinction model."

The significant point here is that the A78 nucleus, in contrast to that of A30, is not very much reddened by circumstellar dust. Yet the infrared fluxes from the two, as shown by CHOS, are quite similar, indicating that the amount of such dust in the two nebulae may be roughly the same. A simple explanation is that the distribution of the dust is different. We conclude that for A78, the dust is arranged in a torus around the star, and that we view it pole-on, whereas we are either looking through the equator of a torus at the A30 nucleus, or that the dust is more spherically distributed. We speculate that this difference might be related to the morphological dissimilarity, where A78 has the more toroidal appearance (see § I).

The corrected mean fluxes are given in column (5) of Table 3, where

$$\log F_\lambda(\text{corr}) = \log F_\lambda(\text{obs}) + 0.164 (f_\lambda + 1) + 0.13 [f_\lambda(\text{A30}) + 1]. \quad (2)$$

The mean observed and corrected fluxes are displayed in Figure 3 by boxes and circles, respectively. The longer wavelength fluxes are replotted at quadruple scale (given by the interior y-axis), for clarity of display. The reader is cautioned here, however, that this is just one of the several choices for extinction; others are discussed in the next subsection.

### c) Stellar Temperature

Once we have dereddened the stellar flux, we should be able to determine a color temperature simply by fitting models to the corrected observations. The photometry and extinction errors can then be used to derive errors to the temperature, once a given model is assumed. There are several models available, but none is wholly satisfactory, as all lack the correct chemical composition, and do not treat properly the expanding atmosphere of the star. We have examined

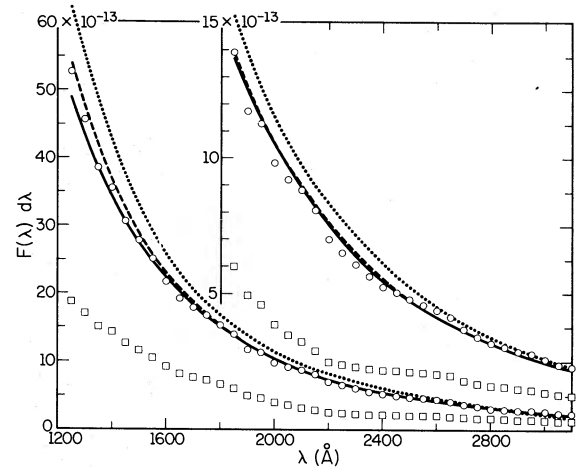


FIG. 3.—The flux distribution in  $\text{ergs cm}^{-2} \text{s}^{-1} \text{\AA}^{-1}$  of the nucleus of Abell 78. The values plotted are a weighted mean of all exposures, excluding the saturated regions in SWP 13351 and LWR 10189. Boxes: the observed fluxes; circles: the fluxes corrected for interstellar extinction, with  $c = 0.164$ ,  $c(\text{A30}) = 0.013$  (see text). Longward of  $\lambda 1800 \text{\AA}$  the points are replotted on a larger scale (relative to the ordinate scale inside the figure) for clarity of display. The curves show model flux distributions scaled to the optical data. Solid line: blackbody fit to the UV data at  $T = 77,000 \text{ K}$ ; dotted line: the Wesemael (1981) line-blanketed helium star model for  $100,000 \text{ K}$ ,  $\log g = 6.0$ ; dashed line: the Wesemael (1981) line-blanketed helium star model for  $70,000 \text{ K}$ ,  $\log g = 8$ , and the Hummer and Mihalas (1970) 200 series model for  $75,000 \text{ K}$ ,  $\log g = 5.5$ , which are indistinguishable on this scale. The dashed line is absent where it is inseparable from the solid line. Note that this is but one possible solution based upon one interpretation of the extinction data: see Table 4.

a number of possibilities in order that we may at least bracket the true temperature, and decide on a particular value.

An obvious choice, of course, is the blackbody. For a given observed energy distribution, this assumption will yield the highest temperature. There is ample justification for its use. First, it is simple, and other models have equally obvious flaws. Second, model calculations by Kunasz, Hummer, and Mihalas (1975), and recent work by Hummer (1983 and private communication), show that the expected energy distribution from a star with an extended or expanding outer atmosphere, implied here by the strong P Cygni profiles, approaches that of a blackbody, as compared to the earlier LTE-plane parallel models of Hummer and Mihalas (1970, hereafter HM). And although the conditions are not entirely comparable, Kaler (1976) found that for the cooler nuclei, the blackbody assumption gave more consistent results than did the HM models. Finally, since the star has no surface hydrogen, as indicated by the nebular helium zones, there are no hydrogen absorption edges to distort the continuum. Since  $\lambda 1640 \text{ He II}$  is not seen and  $\lambda 4686 \text{ He II}$  is weak (CHOS), continuous absorption by  $\text{He}^+$  is probably not important either.

Another obvious choice, of course, is the set of helium model atmospheres by Wesemael (1981). But Wesemael's models are for a pure helium composition, and the line spectrum of the A78 nucleus shows that C, N, and O are present, although to an unknown degree. In addition, the examination by Jacoby and Ford (1983) of nebular material that should be representative of the star shows roughly normal nitrogen, oxygen, and neon to helium ratios. This study also suggests an anomalously high carbon abundance for A30, which by analogy may exist for A78 as well.

We can also use the standard models of HM, but these are for a hydrogen atmosphere of normal composition, and clearly do not relate well to this particular star. They will, however, yield a lower bracketing limit to the effective temperature.

Our fitting procedure for temperature is a variation on that used to determine extinction. The fitting program allows us to fit the data to the theory at any wavelength or over any wavelength interval, and to test the fit over any other wavelength interval that may or may not be coincident with the fitting interval. In order to provide a long wavelength base, we fit the theory to an average of the CHOS and Greenstein (1983) data at  $\lambda\lambda 4400, 5000, 5500, \text{ and } 6600$ , and then tested the goodness of fit by equation (1), using all the points in the interval from  $\lambda 1250$  to  $\lambda 3100$ , plus the five optical points. We then incremented the temperature in the case of the blackbody, or changed the model, in order to find the minimum  $\sum d^2$  (eq. [1]) derived from the points within the testing interval. This will be called the "primary fit"; the effect of varying the fitting and testing intervals will be discussed below.

The extinctions derived in the last subsection, especially that value determined from the optical data, are dependent upon the assumed temperature;  $\bar{c}(\text{optical})$ , for example, changes from 0.163 at 60,000 K to 0.203 at 120,000 K. All solutions described below involved iteration between temperature and extinction. Unless otherwise specified,  $c = c(\lambda 2200)$ , and  $c(\text{A30}) = \bar{c}(\text{optical}) - c(\lambda 2200)$ .

When we assume a blackbody and the basic extinction model as given in subsection *b* and restated above, and increment in units of 1000 K, we find the best fit to occur at 77,000 K, whence the choice for the extinction values in equation (2). This blackbody function is displayed as the solid curve in Figure 3. The overall fit is quite good, as any single point differs from the curve by on the average only 2.9%. Two systematic trends are evident: from  $\lambda 1650$  to  $\lambda 1250$ , the observed flux distribution climbs somewhat faster than that of the theoretical, and in the LWR it ascends rather more slowly. A somewhat similar phenomenon can be seen in the study of the nuclei of NGC 6853 and NGC 7293

by Bohlin, Harrington, and Stecher (1982). Given the differences among the various exposures, and the SWP-LWR match-up problem discussed earlier, both of these effects are small enough to be simply the result of systematic error in observation and reduction.

In order to find likely error limits on the temperature, we must take account of the uncertainties in the extinction and the photometry. A variety of combinations are presented in Table 4, which gives the iterated extinctions,  $c$  and  $c(\text{A30})$ . The first row restates the result for the basic extinction model of § IIIb, with no errors applied. The next two give the color temperatures derived by applying the photometric error as a multiplicative factor to all the UV data ( $\lambda < 3200 \text{ \AA}$ ). The  $\pm 3.5\%$  error translates into a temperature error of about  $\pm 8500 \text{ K}$ .

The lowest extinction derivable from the  $\lambda 2200$  feature [where again  $c(\text{A30}) = \bar{c}(\text{optical}) - c(\lambda 2200)$ ], shown in row (4), easily takes us below the lowest Zanstra temperature of 67,000 K (from Table 1, the formal value minus the error), which we take through this study as the most reasonable lower limit. In the next four rows, we assume that there is no circumstellar extinction, and derive  $T$  for a variety of ways of averaging the interstellar extinction values. In row (5), we average the optical and UV extinctions to find a temperature identical to row (1). In row (6), we assume that  $c(\lambda 2200)$  is erroneously low, and adopt only  $\bar{c}(\text{optical})$ , which is encompassed by the rather large error in  $c(\lambda 2200)$ . We consider this possibility about as likely as our basic extinction model. In row (7), we adopt only the CHOS value of  $c$ , which is the optical upper limit, and which is very close to the  $\lambda 2200$  upper limit. Finally in row (8), we apply both the 3.5% photometric error and the upper  $\lambda 2200$  extinction limit to the data to find a most likely maximum of 130,000 K.

Note that the best fit from the mean percentage error occurs for rows (6) and (7), which give temperatures of 84,000 K and 108,000 K. Thus, there is some marginal evidence that the "basic extinction model" is incorrect, and that the color temperature is larger than given in the first row. Further work is clearly needed on the extinction to the star.

TABLE 4  
BLACKBODY TEMPERATURE AS A FUNCTION OF EXTINCTION AND UV-TO-OPTICAL ERROR

| Model/Combination                                 | $c$   | $c(\text{A30})$ | Error <sup>a</sup> | $T(\text{K})$ | $\overline{PE}(\%)^b$ | $\log L/L_\odot^c$ | Mass ( $M_\odot$ ) <sup>c</sup> |
|---|-------|-----------------|--------------------|---------------|-----------------------|--------------------|---------------------------------|
| A. Savage and Mathis (1979)–Whitford Extinction   |       |                 |                    |               |                       |                    |                                 |
| 1. Basic extinction model (§ IIIb) .....          | 0.164 | 0.013           | 1.00               | 77,000        | 2.9                   | 3.34               | 0.56                            |
| 2. Optical-UV error .....                         | 0.167 | 0.017           | 1.035              | 87,000        | 3.3                   | 3.50               | 0.58                            |
| 3. Optical-UV error .....                         | 0.165 | 0.007           | 0.966              | 70,000        | 3.2                   | 3.22               | 0.55                            |
| 4. Lower limit .....                              | 0.122 | 0.032           | 1.00               | 63,000        | 4.6                   | 3.10               | ~0.54                           |
| 5. Mean optical + $\lambda 2200$ extinction ..... | 0.160 | 0.00            | 1.00               | 77,000        | 2.8                   | 3.34               | 0.56                            |
| 6. Mean optical extinction .....                  | 0.182 | 0.00            | 1.00               | 84,000        | 2.5                   | 3.45               | 0.58                            |
| 7. CHOS only .....                                | 0.211 | 0.00            | 1.00               | 108,000       | 2.5                   | 3.77               | 0.63                            |
| 8. Upper limit .....                              | 0.215 | 0.00            | 1.035              | 130,000       | 3.6                   | 4.01               | ~0.70                           |
| B. Code <i>et al.</i> (1976) Extinction           |       |                 |                    |               |                       |                    |                                 |
| 9. Basic extinction model .....                   | 0.168 | 0.017           | 1.00               | 87,000        | 3.2                   | 3.50               | 0.58                            |
| 10. Lower limit .....                             | 0.123 | 0.033           | 1.00               | 66,000        | 4.2                   | 3.14               | 0.55                            |
| 11. ~ Upper limit .....                           | 0.215 | 0.00            | 1.035              | 154,000       | 4.8                   | 4.21               | ~0.79                           |

<sup>a</sup> Error applied as a multiplicative factor to all the UV data ( $\lambda < 3200 \text{ \AA}$ ).

<sup>b</sup> Mean percentage error computed from all points in the fit.

<sup>c</sup> Based upon the distance in Table 1.

An additional source of error is the reddening function itself, which we have so far taken as fixed. If we use the composite UV extinction function adopted by Code *et al.* (1976) (again joined to the optical Whitford function) and apply all the above procedures, we find the results listed in rows (9), (10), and (11). As before, we can easily reach the Zanstra limit, but now we can push the temperature to over 150,000 K. The extinction in row (11) is derived from the upper limit to  $c(\lambda 2200)$ : if we were to assume a circumstellar extinction of  $c(\text{CHOS}) - c(\lambda 2200)$ , (upper limit), the temperature would go even higher. But note that the fit is generally worse for their reddening function, which argues against it. In addition, it is very unlikely that all the sources of error would act in concert to elevate the temperature in this way, and we still adopt our earlier upper limit of 130,000 K as the most reasonable.

By fitting and testing at other wavelength points or over other intervals, we can give an idea of the goodness of fit between observation and theory, and provide a measure of the error inherent in the method. The results for a variety of choices are summarized in Table 5, all of which assume the basic extinction model. The first row restates the solution for the primary fit. For the next three rows, the fitting interval remains in the optical, but the longward limit to the testing interval progresses steadily toward shorter wavelengths until in row (4), we determine  $T$  only from the extremes,  $F(\lambda 1250)/F(\text{optical})$ . (The error introduced by the uncertainty in the line at  $\lambda 1310$  is of little consequence unless one uses only this latter extreme. If we assume that instead of having a P Cygni profile this line is in pure absorption, then  $T(\lambda 1250/\text{optical})$  is increased from 88,000 K to 93,000 K.) For row (5) we both test and fit over all the data, and for the last two rows we exclude the optical region entirely, and derive  $T$  first from the combined SWP-LWR spectra, and then from the SWP spectrum alone. In these alternative analyses, we see the effects of the systematic trends in Figure 3 discussed above. The variation among the temperatures in Table 5 is less than that produced by varying the extinction between its allowed values, and applying the ultraviolet to optical error of  $\pm 3.5\%$  to the primary fit. The alternative fitting procedures could, if applied to the various assumptions in Table 4, drive the temperature even higher than discussed above. But except for row (5), for which the temperature is similar to that in row (1), all these alternatives ignore useful and pertinent data. We still adopt our primary blackbody fit, with its assigned errors, as best.

We next consider the application of various stellar models,

TABLE 5  
BLACKBODY TEMPERATURES FOR A VARIETY OF FITTING  
AND TESTING INTERVALS

| Fitting Interval                       | Testing Interval              | $T(\text{blackbody})$ (K) |
|--|-------------------------------|---------------------------|
| 1. $\lambda 4400 - \lambda 6600$ ..... | $\lambda 1250 - \lambda 6600$ | 77,000 <sup>a</sup>       |
| 2. $\lambda 4400 - \lambda 6600$ ..... | $\lambda 1250 - \lambda 1800$ | 79,000                    |
| 3. $\lambda 4400 - \lambda 6600$ ..... | $\lambda 1250 - \lambda 1400$ | 82,000                    |
| 4. $\lambda 4400 - \lambda 6600$ ..... | $\lambda 1250$ only           | 88,000                    |
| 5. $\lambda 1250 - \lambda 6600$ ..... | $\lambda 1250 - \lambda 6600$ | 78,000                    |
| 6. $\lambda 1250 - \lambda 3000$ ..... | $\lambda 1250 - \lambda 3000$ | 79,000                    |
| 7. $\lambda 1250 - \lambda 1800$ ..... | $\lambda 1250 - \lambda 1800$ | 104,000                   |

<sup>a</sup> Primary fit (see text).

where we again first fit the predicted fluxes to the optical data, and then compare the agreement between theory and observation throughout the observed spectrum. Although none of the models is entirely appropriate, as discussed earlier, they might at least be used to set some sort of bounds on temperature. From Table 1, we can safely adopt  $\log g = 6.0$  and 5.5 for the Wesemael (1981) line-blanketed helium, and the HM hydrogen models, respectively. The former author's helium star model for 100,000 K, shown by the dotted line in Figure 3, gives an energy distribution that is clearly too steep. Although the surface gravity is unrealistically high, the helium model at 70,000 K,  $\log g = 8$ , shown by the dashed line where it is not inseparable from the solid curve (and where we smooth over the broad He II lines), fits quite well. From the HM models at 75,000 K, 90,000 K, and 100,000 K (models 229, 226, 227), the best fit is for model 229 at 75,000 K. The resulting curve is identical at this level of detail to the dashed curve for the 70,000 K helium model.

In order to be quantitatively more precise, we use the blackbody to interpolate between the models by finding the temperatures at which a blackbody fits the models, in the same manner in which we fit the blackbody to the data. For the HM ( $\log g = 5.5$ ) models,

$$T(\text{model}) = 0.62 T(\text{blackbody}) + 24,000, \quad (3)$$

and from our blackbody fit of 77,000 K, we find an equivalent HM temperature of 72,000 K. The range due to error is again from the Zanstra limit now to 105,000 K. The best blackbody fit to the Wesemael (1981) 100,000 K  $\log g = 6$  model occurs for 120,000 K. Assuming a slope similar to equation (3), for which the last term becomes 26,000 K, we analogously find an equivalent helium model temperature for the basic extinction model of  $\approx 74,000$  K, with a likely maximum of 107,000 K. Neither of the two models represented by the dashed line in Figure 3 fit as well as the blackbody. The average percentage errors for the 70,000 K helium model and the 75,000 K HM model are 0.0355 and 0.0392, respectively; compare with Table 4. These fits could be improved somewhat with models of the proper temperature and gravity. From all the arguments given above (at least until better ones become available), we feel that the blackbody solutions are the most appropriate to the determination of the correct value of effective temperature. Within the 67,000–130,000 K full span, the current best two extinction estimates suggest that the most likely temperature range is 77,000–84,000 K.

As a final comment to this section, we note that KF find that at least for the lower luminosity nuclei without significant winds, the ultraviolet color temperatures inferred by fitting blackbody curves to the observed energy distributions are probably upper limits to the effective temperatures. The same may be true for A78; however, this conclusion may not be transferable to stars with powerful winds and extensive envelopes. In any case, our adopted extreme temperature range already encompasses values upward from the Zanstra limit.

#### d) Discussion

The above analysis lends itself to some brief commentary. The temperature implied by Pottasch *et al.* (1978) of 140,000 K from ANS satellite data is almost certainly too high. We have to employ extreme assumptions to reach it. The flux

distribution measured here is also much closer to a blackbody than that found by those authors.

From the temperature, we can determine the optical depth of the nebula at the  $\text{He}^+$  Lyman limit at  $\lambda 228 \text{ \AA}$ ,  $\tau_0(\text{He}^+)$ . We modified the Zanstra temperature program described by Kaler (1983) to include variable  $\tau_0(\text{He}^+)$ , assuming that  $\tau_v = \tau_0(\text{He}^+)(v/v_0)^{-3}$ . To bring the  $\text{He II}$  Zanstra temperature from its value in Table 1 (calculated under the assumption that  $\tau_0 = \infty$ ) to the 77,000 K value requires that  $\tau_0(\text{He}^+)$  be of the order of 0.4, which is consistent with the fact that helium is dominantly ionized throughout the entire nebula. Consideration of the effects of internal dust would of course raise this figure, and adoption of higher temperatures would lower it.

Iben *et al.* (1983) and Kaler (1983) give a locus on the  $\log L$ - $\log T$  plane along which the A78 nucleus must lie, which terminates at the Zanstra temperature and luminosity. With the higher extinction given in Table 1, this path should be raised upward by 0.08 in  $\log L$ . From the evolutionary tracks of Paczyński (1971) as modified by Iben and Renzini (1982) for  $0.6 M_\odot$  (with the modification scaled to higher masses) and from the  $0.55 M_\odot$  track calculated by Schönberner and Weidemann (1981 and private communication), we can interpolate the mass of the A78 nucleus for any value of temperature. We give these, as well as the luminosities, in the last two columns of Table 4.

In the study by Iben *et al.* (1983), the authors used a preliminary temperature for the A78 nucleus of 100,000 K, derived from the longest SWP + LWR exposures only. This temperature, which is still encompassed by our more refined treatment, indicates a core mass of  $0.6 M_\odot$ , which given their calculated evolutionary time scales, implies independently that the star is now undergoing a second passage through the plane. However, a change to a lower temperature with an allowed range of 67,000–130,000 K renders any conclusions based only upon position on the plane uncertain. At 77,000 K and a core mass of  $0.56 M_\odot$ , the evolutionary time scale of the star is so long (Schönberner 1981; Schönberner and Weidemann 1983) that the nebula would be able to grow to its present size during its first passage. For higher assumed temperature, the likelihood of second passage from this argument continues to grow until it becomes a near certainty near the upper limit. Further progress will require improvement in the precision of the interstellar extinction constant.

Additional uncertainties must be considered that compound the problem. The expansion velocity of the nebula is unknown, and if it is of the order of  $40 \text{ km s}^{-1}$  (see Sabbadin and Hamzaoglu 1982), the nebula would have time to grow to its  $0.43 \text{ pc}$  radius during the first passage at stellar masses somewhat under  $0.58 M_\odot$ . But as we consider expansions below  $20 \text{ km s}^{-1}$ , the likelihood of second passage increases for masses below  $0.6 M_\odot$ . Of even greater importance, however, is the uncertainty in distance. For example, a 50% increase in the distance scale (similar to the Cudworth 1974 system), would yield a core mass of about  $0.58 M_\odot$  even at the lowest Zanstra limit and strengthen the contention of second passage. On the other hand, a decrease in distance by a factor of 2, which would require a factor of 5 reduction in the assumed nebular mass (see Cahn and

Kaler 1971), would place the star on the  $0.55 M_\odot$  track even at a temperature of 94,000 K.

For a final comment, we return to A30. Unfortunately, because of the circumstellar dust, the temperature of that nucleus cannot now be determined. If we apply the same principles of analysis to this star that we used for A78, and employ the Zanstra limits of Table 1, we see that at 81,000 K it would have a mass of only  $0.55 M_\odot$  with its much slower evolutionary rate. In order to attain a mass of  $0.58 M_\odot$ , the temperature would have to be higher, somewhat above 100,000 K, contingent of course upon the accuracy of the adopted distance. We can, however, conclude by analogy with A78 that the circumstellar absorption curve determined for A30 by Greenstein (1981) for 100,000 K is probably more appropriate than the one for 200,000 K.

#### e) Summary

In summary, we are able to draw some conclusions that are quite definite and others that only point the way for future research. The dust distribution around the central star of A78, or at least that in the line of sight, is quite different from that about the A30 nucleus. A toroidal distribution, wherein the dust clouds embedded within A30 and A78 are oriented differently, is a distinct and likely possibility. The temperature of the A78 core is not as high as previously believed, and almost certainly lies between 67,000 K and 130,000 K. On the basis of the best currently available extinctions, the most likely temperatures fall at 77,000 K or 84,000 K. Note again from KF (see the end to § IIIc) that these values be upper limits to the true effective temperature.

At the adopted distance, the full temperature range implies that the core mass lies between  $0.56$  and  $0.70 M_\odot$ , with more likely values between  $0.56$  and  $0.58 M_\odot$ . The uncertainties in temperature, expansion velocity, and distance are such that these data alone, coupled with evolution-time calculations, can neither confirm nor deny the likelihood that the star is now a second passage through the  $\log L$ - $\log T$  plane, a position which is however supported by other observations.

We have made every attempt to provide sufficient information to allow the reader to make an independent judgment, and to allow firmer conclusions to be drawn in the light of subsequent investigations. Further progress must await a better extinction to this particular star, the examination of more stars that may be undergoing a second passage through the  $\log L$ - $\log T$  plane in order that statistical distance methods be more reliable, and the establishment of some individual distances, as well as precise measurement of more effective temperatures. We also must have models that are tailored to the physical and chemical conditions of the star in question.

This work was supported by NASA grant NAG 5-171 and by National Science Foundation grant AST 80-23233, both to the University of Illinois. We would like to thank the *IUE Observatory* staff for their indispensable aid, Drs. J. Greenstein and G. Jacoby for transmitting results in advance of publication, and Drs. Greenstein, D. Hummer, and J. Lutz for helpful commentary.

## REFERENCES

- Adelman, C. J., Adelman, S. J., and Fischel, D. 1977, *Wavelengths and Transition Probabilities for Atoms and Atomic Ions*, NASA Publication X-685-77-287.
- Bohlin, R. C., Harrington, J. P., and Stecher, T. P. 1982, *Ap. J.*, **252**, 635.
- Bohlin, R. C., and Holm, A. 1980, *IUE Newsletter*, No. 10.
- Cahn, J. H., and Kaler, J. B. 1971, *Ap. J. Suppl.*, **22**, 319.
- Code, A. D., Davis, J., Bless, R. C., and Brown, R. H. 1976, *Ap. J.*, **203**, 417.
- Cohen, M., Hudson, H. S., O'Dell, S. L., and Stein, W. A. 1977, *M.N.R.A.S.*, **181**, 233 (CHOS).
- Cudworth, K. M. 1974, *A.J.*, **79**, 1384.
- Greenstein, J. L. 1981, *Ap. J.*, **245**, 124.
- . 1983, private communication.
- Greenstein, J. L., and Minkowski, R. 1964, *Ap. J.*, **140**, 1601.
- Hazard, C., Terlevich, R., Morton, D. C., Sargent, W. L. W., and Ferland, G. 1980, *Nature*, **285**, 463.
- Heap, S. R. 1979, in *IAU Symposium 83, Mass Loss and Evolution of O-Type Stars*, ed. P. S. Conti and C. W. H. de Loore (Dordrecht: Reidel), p. 99.
- Helfer, H. L., Herter, T., Lacasse, M. G., Savedoff, M. P., and van Horn, H. M. 1981, *Astr. Ap.*, **94**, 109.
- Hummer, D. G. 1983, in *IAU Symposium 103, Planetary Nebulae*, ed. D. Flower (Dordrecht: Reidel), p. 211.
- Hummer, D. G., and Mihalas, D. 1970, *JILA Report 101* (HM).
- Iben, I., Jr., Kaler, J. B., Truran, J. W., and Renzini, A. 1983, *Ap. J.*, **264**, 605.
- Iben, I., Jr., and Renzini, A. 1982, Illinois Astrophysical Preprint IAP82-2.
- Jacoby, G. H., and Ford, H. A. 1983, *Ap. J.*, **266**, 298.
- Kaler, J. B. 1976, *Ap. J.*, **210**, 843.
- . 1981, *Ap. J. (Letters)*, **250**, L31.
- . 1983, *Ap. J.*, **271**, 188.
- Kaler, J. B., and Feibelman, W. A. 1984, *Ap. J.*, submitted (KF).
- Kelly, R. L. 1979, NASA TM-80268.
- Kunasz, P. B., Hummer, D. G., and Mihalas, D. 1975, *M.N.R.A.S.*, **202**, 92.
- Oke, J. B., and Gunn, J. E. 1983, *Ap. J.*, **266**, 713.
- Paczynski, B. 1971, *Acta Astr.*, **21**, 417.
- Perek, L., and Kohoutek, L. 1967, *Catalogue of Galactic Planetary Nebulae*, (Prague: Czechoslovakia Academy of Sciences).
- Pottasch, S. R., Wesselius, P. R., Wu, C.-C., Fieten, H., and van Duinen, R. J. 1978, *Astr. Ap.*, **62**, 95.
- Reay, N. K., Atherton, P. D., and Taylor, K. 1983, in *IAU Symposium 103, Planetary Nebulae*, ed. D. Flower (Dordrecht: Reidel), p. 508.
- Sabbadin, F., and Hamzaoglu, E. 1982, *Astr. Ap.*, **110**, 105.
- Savage, B. D., and Mathis, J. S. 1979, *Ann. Rev. Astr. Ap.*, **17**, 73.
- Schönberner, D. 1981, *Astr. Ap.*, **103**, 119.
- Schönberner, D., and Wiedemann, V. 1981, *Physical Processes in Red Giants*, ed. I. Iben, Jr. and A. Renzini (Dordrecht: Reidel), p. 463.
- . 1983, *IAU Symposium 103, Planetary Nebulae*, ed. D. Flower (Dordrecht: Reidel), p. 359.
- Wesemael, F. 1981, *Ap. J. Suppl.*, **45**, 177.
- Whitford, A. E. 1958, *A.J.*, **63**, 201.

NOTE ADDED IN PROOF.—H. L. Dinerstein and D. F. Lester (1984, *Ap. J.*, **281**, 702) find evidence for a dusty disk in front of the central star of Abell 30, but these authors (private communication) do not see a similar concentration in front of the Abell 78 nucleus, consistent with our determination of very low circumstellar extinction.

JAMES B. KALER: Department of Astronomy, University of Illinois, Room 341, Astronomy Building, 1011 West Springfield Avenue, Urbana, IL 61801

WALTER A. FEIBELMAN: Laboratory for Astronomy and Solar Physics, NASA/Goddard Space Flight Center, Greenbelt, MD 20771